J Solid State Electrochem (2012) 16:1313–1321
DOI 10.1007/s10008-011-1524-3

ORIGINAL PAPER

Facile synthesis of ultra-long Cu microdendrites for the electrochemical detection of glucose

De-Jun Chen · Ya-Hui Lu · Ai-Jun Wang · Jiu-Ju Feng · Tian-Tian Huo · Wen-Ju Dong

Received: 11 July 2011 / Revised: 3 August 2011 / Accepted: 4 August 2011 / Published online: 18 August 2011

Abstract Ultra-long Cu microdendrites (MDs) were prepared by one-step electrodeposition on a glassy carbon electrode. The results demonstrated that the reduction potential, pH, and temperature of the electrolysis solution, as well as the amount of Cu^{2+} and citrate ions, play important roles in the formation of the Cu MDs. Notably, the X-ray diffraction experiments confirmed that the aggregations of the Cu nanocrystals preferred to grow along (111) direction. In addition, the resulting Cu MDs-modified electrode showed good electrochemical performance as a non-enzyme glucose sensor in alkaline media.

Keywords β-*D*-Glucose · Cu microdendrites · Electrodeposition · Electrocatalysis

Introduction

Metals, with unique physical and chemical properties, have wide applications in fuel cells, sensors, and electronic devices [1–8]. Among them, Cu is attractive due to its low cost, compared to noble metals. More importantly, Cu has additional advantages [9]: (1) good catalyst for many different reactions, (2) convenient material for electrochemical reactions since it can be directly electrodeposited on an electrode surface in a simple way, and (3) without extra chemical treatment or special techniques to affix the catalyst onto the electrode surface.

Recently, synthesis of different metallic nanostructures becomes a hot subject for its broad applications in catalysis, biological labeling, optoelectronics, and surface-enhanced Raman fields [10–13]. Specifically, dendritic materials, consisting of a main stem and numerous side branches, receive significant attention in catalysis and technological fields [14–21, 23]. For example, Fang and coworkers [18] prepared the nanoparticle-aggregated three-dimensional monocrystalline Au nanodendrites. In another example, Zhang and his coworkers [22] fabricated Cu dendritic nanostructures.

Electrodeposition is always popular for the synthesis of dendritic materials, which is mainly ascribed to its facile operation, precise control, low cost, being benign to environment, and good repeatability [22–24]. Moreover, straightforward formation of metal nanostructures on a variety of substrates can be easily employed as electronic or optic devices [2, 25]. For instance, Choi et al. [20] reported the electrosynthesis of porous dendritic Cu fibers. Besides, Shao and Zangari electrodeposited Cu dendrites on silicon surface from an acidic sulfate electrolyte [26]. Lately, Kang and his coworkers simply constructed Cu [27] and Cu–Ni hybrid dendrites [28] on Cu foils by a one-step amperometric technique. As known, metallic dendrites are easy to grow on the same metal substrates [27, 28] or ITO glass [29]. Conversely, on foreign substrates, such as glassy carbon electrodes (GCE), generation of uniform and well-defined metal structures at a large scale is still challenging.

Electronic supplementary material The online version of this article (doi:10.1007/s10008-011-1524-3) contains supplementary material, which is available to authorized users.

D.-J. Chen · Y.-H. Lu · A.-J. Wang · J.-J. Feng (✉) · T.-T. Huo · W.-J. Dong
Key Laboratory of Green Chemical Media and Reactions, Ministry of Education, Henan Normal University, Xinxiang 453007, China
e-mail: jjfeng@zjnu.cn

J.-J. Feng
e-mail: jjfengnju@gmail.com

A.-J. Wang · J.-J. Feng
College of Chemistry and Life Science, College of Geography and Environmental Science, Zhejiang Normal University, Jinhua 321004, China

Here, single crystalline and ultra-long Cu MDs were prepared on the GCE by one-step electrodeposition. The effects of the electrodeposition potential, pH, and temperature of the electrolysis solution and the amount of Cu^{2+} and citrate ions were investigated in some detail. In addition, the Cu MDs-modified electrodes were tested by constructing a non-enzyme glucose sensor with good electrochemical performance.

Experimental

Chemicals and materials

Copper (II) chloride dihydrate ($CuCl_2\,2H_2O$), tri-sodium citrate (Na_3–citrate), sodium dodecyl sulfate (SDS), and β-D-glucose were purchased from Beijing Chemical Plant (Beijing, China). The other chemicals were of analytical grade and used as received. All aqueous solutions were prepared with twice-distilled water.

Apparatus

Scanning electron microscopy images (SEM) were recorded from a JSM-6390LV microscope (JEOL). X-ray diffraction (XRD) analysis was performed with a Rigaku Dmax-2000 diffractometer using CuKα radiation. Electrochemical experiments were conducted on a CHI 660D electrochemical workstation (Shanghai Chenhua, Shanghai, China). All experiments were performed using a conventional three-electrode system, where the GCE was used as the working electrode, a platinum wire as the counter-electrode, and a saturated calomel electrode as the reference electrode. Electrochemical impedance spectroscopy experiments were carried out in 0.1 M KNO_3 solution containing 5.0 mM $Fe(CN)_6^{3-}/Fe(CN)_6^{4-}$ (1 1) at room temperature, using an alternating current voltage of 5.0 mV. The open circuit potential was about 180 mV in the frequency range of 10^{-2}–10^5 Hz.

Preparation of the Cu MDs

Prior to modification, a GCE was polished with a sand paper, followed by 1.0, 0.3, and 0.05 μm alumina powder, cleaned in an ultrasonic bath, and dried in nitrogen. Electrodeposition was performed potentiostatically until the electrode surface was fully covered with the Cu deposits under different potentials (−0.45 to −0.90 V) and temperature (40–80 °C). A 10-mL mixture solution (pH 2.6–6.5) was used here for electrolysis, containing 5.0–160.0 mM $CuCl_2$, 0.0–160.0 mM Na_3–citrate, 20.0 mM glucose, and 0.05 wt.% SDS. Then, the SDS was removed from the electrode surface by thoroughly washing with ethanol and water, respectively. Afterwards, the catalytic ability of the as-prepared Cu deposit was checked for glucose oxidation using 0.1 M NaOH as the electrolyte at room temperature. Finally, a non-enzyme glucose sensor was constructed based on the electrodeposition of the Cu MDs.

Results and discussion

Morphological characterization

Figure 1A shows a typical SEM image of the Cu deposits obtained under standard conditions as mentioned in the "Experimental" section (by using an electrodeposition potential of −0.65 V, a reaction temperature of 60 °C, a reaction time of 210 s, 0.05% SDS, pH 2.7, $[Cu^{2+}]$= 50.0 mM, [citrate]=5.0 mM, [glucose]=20.0 mM). The image reveals the formation of Cu MDs with long stems of up to tens of micrometers. The angles between its main stem and side branches are ca. 60°, suggesting a well-defined correlation between the crystallographic directions of the side branches. The space between the side branches is much larger than those of the Cu nanodendrites prepared previously [27]. Additionally, nearly no secondary branches were observed on the second long main stem. These results

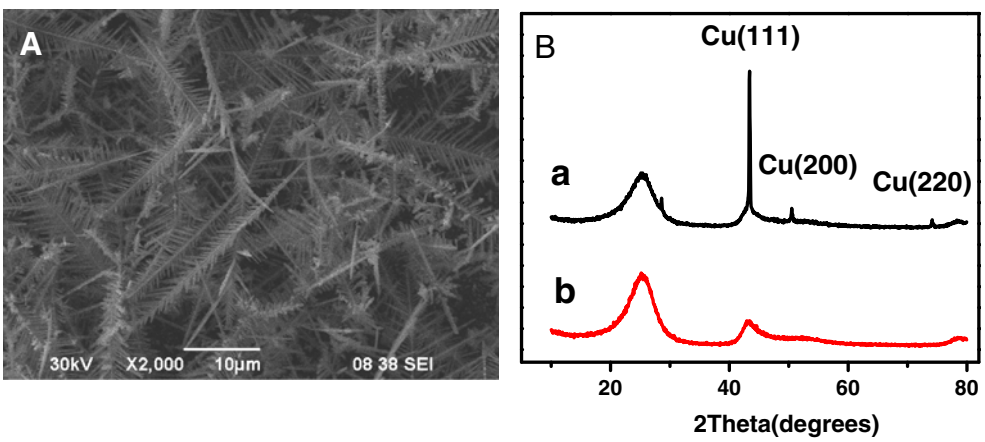

Fig. 1 **A** Typical SEM image of the Cu MDs obtained under standard conditions. **B** XRD patterns of the bare (*b*) and the Cu MDs-modified (*a*) GCE

demonstrate the single-stem-shaped structures of the Cu crystals.

Crystallographic analysis

The obtained Cu MDs were further characterized by XRD experiments to confirm the crystal structures (Fig. 1B). The peaks locate at 43.3°, 50.4°, and 74.2°, which are indexed to the cubic Cu crystal planes of (111), (200), and (220), respectively [22]. Particularly, the intensity of the Cu (111) plane is especially strong and sharp compared to that of the (200) or (220) plane. These results show a good crystal orientation of the Cu MDs, although there is a very weak Cu_2O peak at 28.6° due to the oxidation of Cu itself.

This observation is quite different from those of the Cu and CuNi nanodendrites formed in 0.1 M $CuCl_2$, containing 0.1 M Na_2SO_4 and 0.1 M $Na_2SO_4/NiSO_4$, respectively [30]. In their cases, many higher-order branches were detected. As known, the different surface energy of every crystallographic plane determines the morphology of the final deposits in electrocrystallization [31]. Generally, fast growth rates on a high energy plane leads to large areas of the low energy facets. Nevertheless, the adsorbed molecules or ions have great effects on the surface energy of the crystallographic planes. For instance, sulfate and nitrate anions preferentially adsorb on (111) and (100) planes, consequently slowing the growth rate on these planes, respectively. Moreover, SDS tends to adsorb on the (111) plane, leading to a lower energy than the (100) plane, and thereby the crystals are characterized by the (111) plane. In addition, the adsorption of SDS is affected by pH, and hence intermediate behavior can be observed by decreasing the pH. In our study, both SDS and citrate determine the morphology of the final deposits, which would be discussed later.

Effects of the Cu^{2+} ion concentration

To study the growth mechanism of the Cu MDs, control experiments were performed by changing the amount of Cu^{2+} ion within 5.0–160.0 mM, while the other conditions were unchanged (Fig. 2). Using 5.0 mM Cu^{2+} ion (Fig. 2A), some small grains and Cu MDs with tiny stems were observed. With 40 mM Cu^{2+} ion, many thick stems of the Cu MDs were obtained. When the Cu^{2+} ion concentration is 50.0 mM, a lot of well-defined Cu MDs appeared (Fig. 1A). However, with a continual increase of Cu^{2+} ion concentration up to 80.0 mM, some infant Cu MDs, nanocrystal seeding, and stem-like junctions were detected (Fig. 2C). When the concentration is 160.0 mM, only a compact layer of Cu nanoparticles was observed (Fig. 2D). It is due to the inefficient coordination of the citrate anion with the Cu^{2+} ion.

By analyzing the experimental results, we provide the corresponding voltammetric curves (Electronic supplementary materials, Fig. S1A). There are two well-defined cathodic peaks of the Cu_2O and Cu at −0.22 and −0.36 V, respectively. With the increase of the Cu^{2+} ion, both peaks gradually shifted to a more negative potential. When the Cu^{2+} ion was within 40.0–50.0 mM, the onset potential for the formation of Cu is close to the electrodeposition potential (−0.65 V), leading to the formation of perfect dendrites. These observations are further confirmed by the corresponding *i–t* curves (Fig. 3A). A small amount of Cu^{2+} ions (i.e., 5.0 mM) results

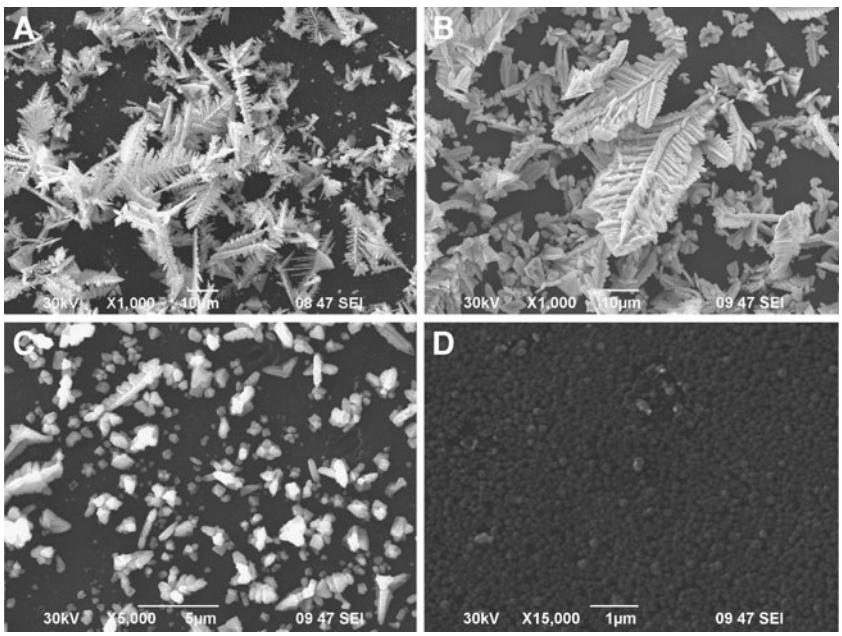

Fig. 2 SEM images of the Cu deposits obtained using different Cu^{2+} ion concentrations: 5.0 mM (**A**), 40.0 mM (**B**), 80.0 mM (**C**), and 160.0 mM (**D**)

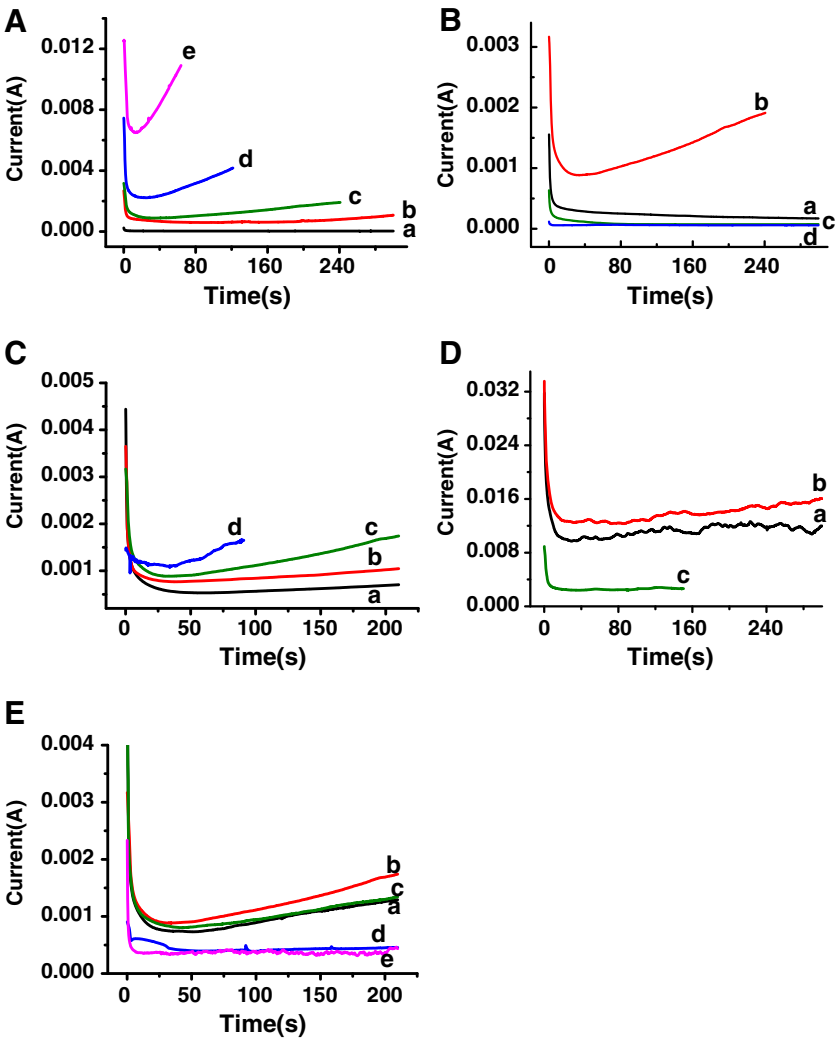

Fig. 3 Chronoamperograms recorded during the electrolysis process. **A** Effect of the Cu^{2+} ion concentration: 5.0 mM (*a*), 40.0 mM (*b*), 50.0 mM (*c*), 80.0 mM (*d*), and 160.0 mM (*e*); **B** effect of the citrate concentration: 2.5 mM (*a*), 5.0 mM (*b*), 20.0 mM (*c*), and 160.0 mM (*d*); **C** effect of the temperature: 40 °C (*a*), 50 °C (*b*), 60 °C (*c*), and 80 °C (*d*); **D** effect of the electrodeposition potential: −0.45 V (*a*), −0.65 V (*b*), and −0.90 V (*c*); **E** effect of the pH: 2.6 (*a*), 2.7 (*b*), 2.8 (*c*), 4.9 (*d*), and 6.5 (*e*)

in lower currents, implying a slower nucleation process. As a result, irregular and large structures were produced. However, more Cu^{2+} ions (i.e., $[Cu^{2+}]$=80.0–160.0 mM) would result in the Cu^{2+} ions being partly uncomplexed, definitely leading to the morphology change of the final deposits. Since a too fast nucleation process would generate a high density of seed crystals and thereby produce small nanostructures, 50.0 mM of the Cu^{2+} ion was therefore chosen as the optimal concentration in the following experiments.

Effect of the citrate concentration

As discussed before, citrate strongly coordinate with Cu^{2+} ion to form the Cu^{2+}–citrate complex. It also acts as a capping agent to protect the newly formed Cu nuclei [32]. Selective adsorption and desorption of the citrate on certain crystal planes have a direct effect on the anisotropic growth of the Cu crystals.

We performed the experiments by adjusting the amount of citrate, while the other conditions were kept constant (Electronic supplementary materials, Fig. S2). When the citrate concentration is 2.5 mM, irregular Cu nanostructures were formed, including many seeding nanocrystals, dendritic-like junctions, and nanoparticles. However, the Cu MDs are rarely observed (Electronic supplementary materials, Fig. S2A). A slow nucleation rate allows the nucleation and growth process to coexist for a relatively long time. At a long reaction time, Ostwald ripening can also affect the final morphology of the deposits. When the citrate concentration is 5.0 mM, the perfect Cu MDs with distinct side branches are clearly observed (Fig. 1A). When the amount of the citrate changed from 20.0 mM (Electronic supplementary materials, Fig. S2B) to 160.0 mM (Electronic supplementary materials, Fig. S2C), only a compact layer of monodisperse small particles was obtained, accompanied by a decrease in particle size. Here, each crystal plane is equally covered by citrate anion, resulting in the formation of quasi-spherical particles. These results are similar to that of the Ag nanowires using PVP as a capping agent [33–35].

Our assumption is demonstrated by the corresponding voltammetric (Electronic supplementary materials, Fig. S1B)

and *i–t* (Fig. 3B) curves. Obviously, when the citrate concentration is 5.0 mM, the differences between the onset and electrodeposition potential are the smallest, where the cathodic peak current is the largest for the formation of the Cu deposits. Thus, 5.0 mM is chosen as the optimal concentration for the citrate anions.

Effect of the reaction temperature

We studied the influence of the reaction temperature on the morphology of the Cu deposits, while other conditions were kept constant (Fig. 4). At a low temperature such as 40 °C, there are many seeding crystals and dendritic-like junctions (Fig. 4A). When the temperature is 50 °C, some irregular and smaller Cu MDs are emerged. Particularly, some branched crystal growths were clearly detected (Fig. 4B). The uniform Cu MDs become dominant at 60 °C (Fig. 1A). However, most of the branches disappeared from the main stems at 80 °C, resulting in some sparse main stem with fishbone-like structures (Fig. 4C). Furthermore, some irregular particles were also detected. In addition, the corresponding *i–t* curves were provided for a comparative study (Fig. 3C).

Effect of the electrodeposition potential

The electrodeposition potential, correlated with the overpotential, also affects the size and shape of the Cu deposit, particularly for cathodic deposition [22]. We performed control experiments by changing the electrodeposition potential under other identical conditions. The formation of the Cu deposits occurs when the electrodeposition potential is below −0.36 V. At −0.45 V (Fig. 5A), the Cu MDs formed were short and sparse, compared to that produced under standard conditions (Fig. 1A). However, when the electrodeposition potential was far from the onset potential (i.e.,−0.90 V; Fig. 5B), there were many main stems observed, accompanied by the disappearance of the Cu MDs. Clearly, the branches of the Cu MDs are apart from the main stem, whose size is similar to the main stem. These results illustrate that a more negative potential is not good to form the Cu MDs. In this case, we present the corresponding *i–t* curves for a comparative study (Fig. 3D). Once the electrodeposition potential changes from −0.45 V to −0.60 V, the currents increase accordingly (Fig. 3D, curves a and b). With the growth time elapsing, the Cu MDs continually grow and the side branches develop at the apexes of the crystals, which penetrate the diffusion layer to get the mass transfer to support further growth. The assumption is demonstrated by the SEM results under standard conditions. However, when the potential negatively shifted, the current decreased and thereby the acquired curve became flat (Fig. 3D, curve c), in agreement with the SEM results where only the main stems left and the side branches disappeared. Taken altogether, −0.65 V was selected as the optimal electrodeposition potential.

Effect of the pH in the electrolysis solution

The pH of the electrolysis solution greatly affects the morphology of the final Cu deposits since changing the pH

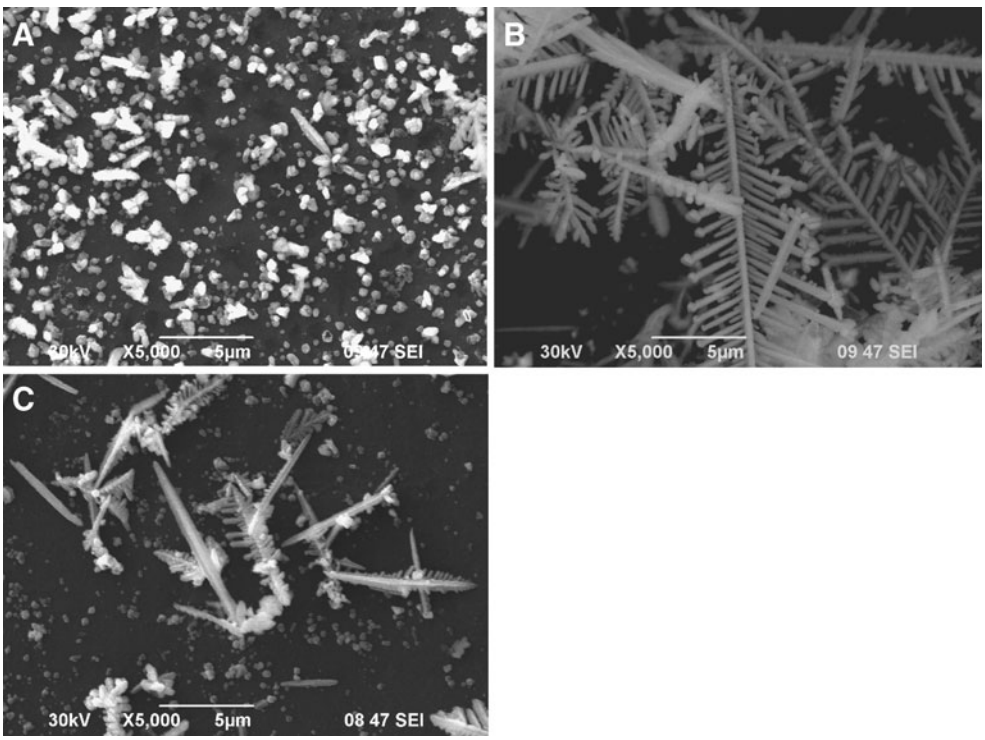

Fig. 4 SEM images of the Cu nanostructures obtained at different reaction temperature: 40 °C (**A**), 50 °C (**B**), and 80 °C (**C**)

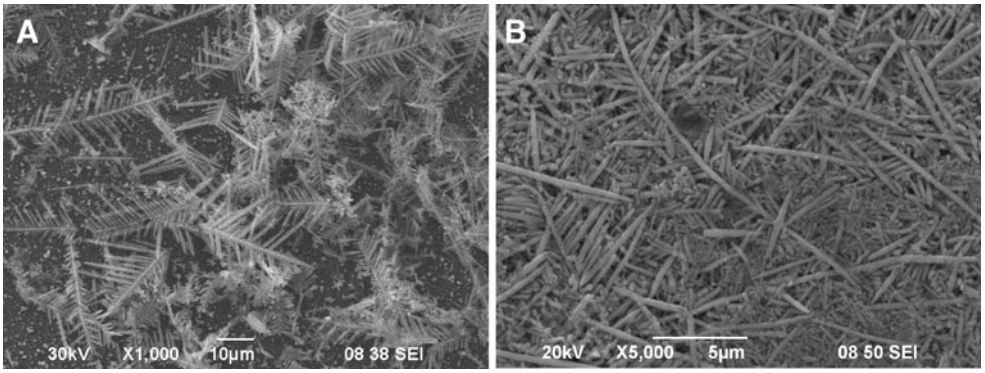

Fig. 5 SEM images of the Cu nanostructures obtained at different electrodeposition potentials: −0.45 V (**A**) and −0.90 V (**B**)

has a great effect on the nucleation and growth rates of the Cu crystal, as well as on the ratio of the deprotonated citrate. As known, increasing the pH would cause the acceleration of the reduction [36]. Furthermore, adjusting the pH also affects the complex equilibrium between the protonated and deprotonated forms of the citrate because different binding affinities to the Cu particle surface were observed for different citrate forms [37]. In addition, changing the pH also influences the onset potential of the Cu crystals.

Herein, the pH control experiments were performed in the pH range of 2.6–6.5 (Electronic supplementary materials, Fig. S3). At low pH such as pH 2.6, a few small Cu MDs in an early form were observed, and some crystals were decorated on the electrode surface (Electronic supplementary materials, Fig. S3A). These observations are different from the Cu MDs obtained under standard conditions (pH 2.7; Fig. 1A). At high pH, for example, pH=4.9 (Electronic supplementary materials, Fig. S3C), only some embryonic forms of the MDs appeared. With further increase in the pH to 6.5, a compact layer of the Cu nanoparticles was observed (Electronic supplementary materials, Fig. S3D). Voltammetric (Electronic supplementary materials, Fig. S1C) and *i*–*t* (Fig. 3E) curves were presented for further characterization. Evidently, at pH 2.7, the onset potential is very close to the electrodeposition potential, accompanied by larger cathodic peak currents for the formation of the Cu crystals, which resulted in well-defined Cu MDs (Fig. 1A). In addition, the trend about the decrease of Cu^{2+} ions with the pH becomes a minor part, from the thermodynamic data and calculated distribution of the species including the amount of citrate, Cu^{2+} ions, and different pH values [32, 33]. Therefore, the pH of 2.7 was chosen as the optimal pH for the electrolysis solution.

Electrochemical impedance spectra of the Cu MD-modified electrodes

The formation of Cu MDs was also monitored by electrochemical impedance spectroscopy (Electronic supplementary materials, Fig. S4). In general, Nyquist plots present the typical features of an electrochemical cell where polarization comes from a combination of electron transfer and diffusion processes (i.e., a semicircle and a linear part, respectively). The formation of the Cu MDs on the GCE results in a drastic increase in the electron transfer resistance, as indicated by a larger diameter of the semicircle in the Nyquist plot (Electronic supplementary materials, Fig. S4, curve b), compared with that of the bare GCE (Electronic supplementary materials, Fig. S4, curve a). This resulted in Cu MDs, as a barrier, blocking the interfacial electron transfer. Thus, the electrochemical behavior of the $[Fe(CN)_6]^{4-/3-}$ probe is controlled by the diffusion and electrochemical reaction together [22].

Practical applications

Linear sweep voltammograms (LSVs) were recorded in 0.1 M NaOH solution to evaluate the electrochemical oxidation of glucose on the Cu MD electrodes at room temperature. Neither oxidation peaks nor catalytic currents were observed at the bare GCE in the presence of 0.8 mM glucose (Fig. 6, curve c). A similar observation was obtained at the Cu MD electrode in a blank solution (Fig. 6, curve b). However, after the addition of 0.8 mM glucose, large catalytic currents were observed at the Cu MD electrodes with an onset potential of 0.25 V (Fig. 6, curve a). Evidently, the Cu MDs can be effectively used as a platform for the detection of glucose.

The electrooxidation currents of glucose at the Cu MD electrodes were tested under different potentials and 0.40 V

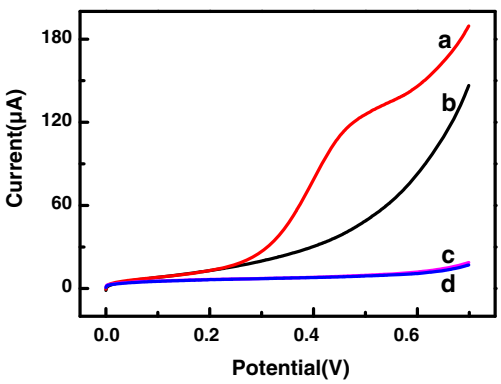

Fig. 6 LSVs of the Cu MDs electrodes (*a* and *b*) and bare GCE (*c* and *d*) in the absence (*b* and *d*) and presence (*a* and *c*) of 0.8 mM glucose at 50 mV s^{-1}

was found as the optimum potential in our study (Electronic supplementary materials, inset in Fig. S5). This value is similar to that of the pillar-like-structured Cu film [38] and more negative than that of 0.65 V [38, 39] or 0.55 V [40] at Cu-based electrodes, respectively. These results suggest a preferable catalytic activity towards glucose at the Cu MD electrode.

Moreover, the catalytic abilities of the deposits prepared under a variety of electrodeposition conditions (including the Cu^{2+} ion concentration, temperature, citrate concentration, and pH of the electrolysis solution) were compared (Fig. 7). Obviously, the well-defined Cu MDs have the strongest catalytic activity, which were prepared through a typical process (by using an electrodeposition potential of −0.65 V, reaction temperature of 60 °C, reaction time of 210 s, 0.05% SDS, pH 2.7, [Cu^{2+}]=50.0 mM, [citrate]=5.0 mM, [glucose]=20.0 mM). The catalytic currents linearly increase with glucose (Fig. 8; the inset figure shows the plot of the peak current vs. glucose concentration, correlation coeffi-

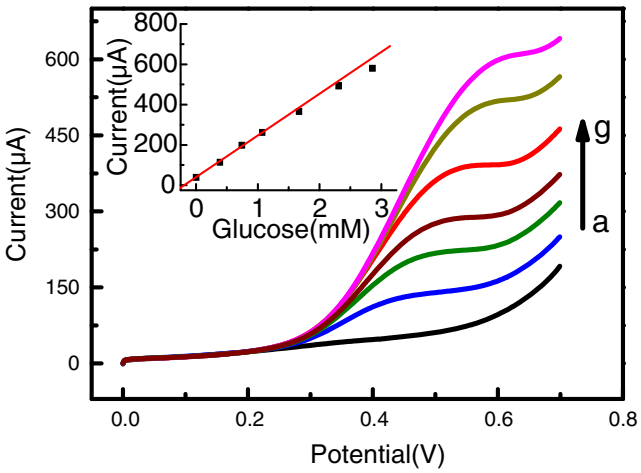

Fig. 8 LSVs of the Cu MDs electrode without (*a*) and with 0.4 mM (*b*), 0.7 mM (*c*), 1.1 mM (*d*), 1.7 mM (*e*), 2.3 mM (*f*), and 2.9 mM (*g*) glucose in 0.1 M NaOH at 50 mV s^{-1}. The *inset* shows the plot of the peak current vs. glucose concentration

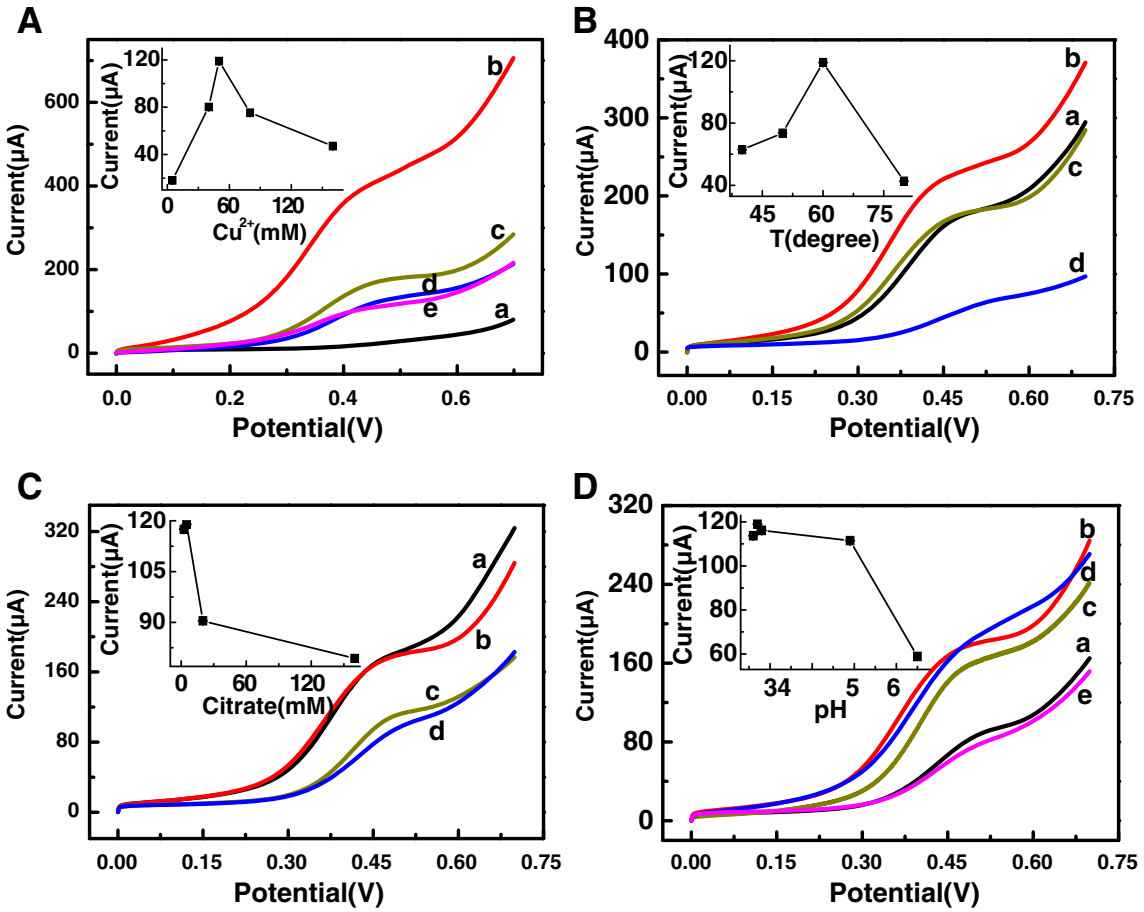

Fig. 7 LSVs of the Cu nanostructure-modified electrodes obtained in the presence of 6 μM glucose at 50 mV s^{-1}. **A** With different Cu^{2+} ion concentration: 5.0 mM (*a*), 40.0 mM (*b*), 50.0 mM (*c*), 80.0 mM (*d*), and 160.0 mM (*e*); the *inset* shows the plot of the peak current vs. concentration of the Cu^{2+} ion. **B** With different electrolysis temperature: 40 °C (*a*), 50 °C (*b*), 60 °C (*c*), and 80 °C (*d*); the *inset* shows the plot of the peak current vs. electrolysis temperature. **C** With different citrate concentration: 2.5 mM (*a*), 5.0 mM (*b*), 20.0 mM (*c*), and 160.0 mM (*d*); the *inset* shows the plot of the peak current vs. citrate concentration. **D** With different pH of the electrolyte: 2.6 (*a*), 2.7 (*b*), 2.8 (*c*), 4.9 (*d*), and 6.5 (*e*); the *inset* shows the plot of the peak current vs. pH of the electrolyte

cient, R=0.9986). Thus, the Cu MDs can facilitate electron transfer and further improve the catalytic ability towards glucose oxidation.

The typical *i–t* curves towards glucose oxidation were recorded at the Cu MD electrode (Electronic supplementary materials, Fig. S5). After an injection of some glucose into a blank solution, the catalytic current reached 90% of the maximum, which was below 3 s. This value is similar to that of the pillar-like-structured Cu film [38] and smaller than that of the Cu nanocubes on the multi-walled carbon nanotube arrays with a value of 5 s [41]. Moreover, the detection limit is 1.4 μM (S/N=3), smaller than that of the Cu nanobelt and Cu–CuO nanowire-modified electrodes with a value of 10 μM [42] and 0.05 mM [43], respectively. The linear range is ranging from 1.4 μM to 3.8 mM, much broader than those of the pillar-like Cu nanostructures [38], Cu nanoblets [42], Cu nanocluster/MWCNTs [44], and Cu nanoparticles/ZnO composite-modified [45] electrodes with a glucose range of 1.0 μM–0.4 mM, 10.0 μM–1.1 mM, 0.7 μM–3.5 mM, and 1.0 μM–1.5 mM, respectively.

Some interfering species usually coexist with glucose in biological samples such as human blood. Thus, it is necessary to check whether these interferents generate current responses comparable to that of glucose or not. The effects of different interferents were tested with the optimal potential of 0.40 V in 0.1 M NaOH containing 4.0 mM glucose. As shown in Table S1 (Electronic supplementary materials), ascorbic acid, catechol, dopamine, and L-glutathione have unnoticeable effect on glucose detection at the interferential ratio of 50, 30, 30, and 10 times of glucose, respectively. The results are consistent with those at the Cu/MWCNT-modified electrode [41, 42] and further illustrate the present method with good selectivity and wide applications for the determination of glucose in biological samples.

In addition, the Cu MDs-modified can be reused several times with reproducible response. For example, five successive measurements with the same electrode showed a dispersion of 3.6% for a given glucose concentration. Long-term stability was also acceptable due to the good stability of Cu itself. After a storage period of 4 weeks in ethanol at 4 °C, the amperometric responses were found to be above 95% of their initial values. The reproducibility was better than 92%, as judged from the amperometric responses of the five electrodes prepared independently.

Conclusions

A simple and low-cost method was developed for the Cu MDs generated on the GCE, which is closely related with the amount of citrate and Cu^{2+} ion, applied potential, reduction temperature, and the pH in the electrolysis solution. The as-prepared Cu MDs demonstrate as a powerful platform for the construction of a non-enzyme sensor with good electrochemical behavior. The present sensor is comparable to that of more complex sensors based on Cu nanostructures or even on the intrinsically more efficient glucose oxidase.

Acknowledgments This work was financially supported by the Natural Science Foundation of China (Nos. 20805011, 20905021).

References

1. Feng J-J, Hildebrandt P, Murgida D (2008) Langmuir 24:1583–1586
2. Feng J-J, Gernert U, Sezer M, Kuhlmann U, Murgida D, David C, Richter M, Knorr A, Hildebrandt P, Weidinger I (2009) Nano Lett 9:298–303
3. Feng J-J, Gernert U, Hildebrandt P, Weidinger IM (2010) Adv Funct Mater 20:1954–1961
4. Chen C, Loo J, Deng M, Kox R, Huys R, Bartic C, Maes G, Borghs G (2010) J Phys Chem C 113:5472–5477
5. Caruso F, Caruso RA, Möhawald H (1998) Science 282:1111–1114
6. Sun Y, Xia Y (2002) Science 298:2176–2179
7. Yang HG, Zeng HC (2004) Angew Chem Int Ed 43:5930–5933
8. Chen J, Saeki F, Wiley BJ, Cang H, Cobb MJ, Li Z-Y, Au L, Zhang H, Kimmey MB, Li X, Xia Y (2005) Nano Lett 5:473–477
9. Feng J-J, Hildebrandt P, Murgida DH (2008) Langmuir 24:1583–1586
10. Murgida DH, Hildebrandt P (2001) J Am Chem Soc 123:4062–4068
11. Mroginski MA, Murgida DH, Hildebrandt P (2007) Acc Chem Res 40:258–266
12. Feng J-J, Hildebrandt P, Murgida DH (2008) Langmuir 24:1583–1586
13. Feng J-J, Lu Y-H, Gernert U, Hildebrandt P, Murgida DH (2009) J Phys Chem C 114:7280–7284
14. Yan H, He R, Johnson J, Law M, Saykally RJ, Yang P (2003) J Am Chem Soc 125:4728–4729
15. Cao M, Liu T, Gao S, Sun G, Wu X, Hu C, Wang ZL (2005) Angew Chem Int Ed 44:4197–4201
16. Shin H, Liu M (2005) Adv Funct Mater 15:582–586
17. Qiu R, Zhang XL, Qiao R, Li Y, Kim YI, Kang YS (2007) Chem Mater 19:4174–4180
18. Fang J, Ma X, Cai H, Song X, Ding B (2006) Nanotechnology 17:5841
19. Wen X, Xie Y-T, Mak WC, Cheung KY, Li X-Y, Renneberg R, Yang S (2006) Langmuir 22:4836–4842
20. Choi K-S (2006) Langmuir 22:10625–10629
21. Panda BR, Rao PN, Paul A, Chattopadhyay A (2006) J Phys Chem B 110:22917–22922
22. Zhang X, Wang G, Liu X, Wu H, Fang B (2008) Cryst Growth Des 8:1430–1434
23. Yu P, Qian Q, Wang X, Cheng H, Ohsaka T, Mao L (2010) J Mater Chem 20:5820–5822
24. Shin H, Dong J, Liu M (2003) Adv Mater 15:1610–1614
25. Feng J-J, Hildebrandt P, Murgida DH (2008) Langmuir 24:1583–1586
26. Shao W, Zangari G (2009) J Phys Chem C 113:10097–10102
27. Qiu R, Cha HG, Noh HB, Shim YB, Zhang XL, Qiao R, Zhang D, Kim YI, Pal U, Kang YS (2009) J Phys Chem C 113:15891–15896
28. Qiu R, Zhang XL, Qiao R, Li Y, Kim YI, Kang YS (2007) Chem Mater 19:4174–4180

29. Armstrong NR, Veneman PA, Ratcliff E, Placencia D, Brumbach M (2009) Acc Chem Res 42:1748–1757
30. Qiu R, Cha HG, Noh HB, Shim YB, Zhang XL, Qiao R, Zhang D, Kim YI, Pal U, Kang YS (2009) J Phys Chem C 113:15891–15896
31. Li C, Shuford KL, Park QH, Cai W, Li Y, Lee EJ, Cho SO (2007) Angew Chem Int Ed 46:3264–3268
32. Zhang H, Xu J-J, Chen H-Y (2008) J Phys Chem C 112:13886–13892
33. Wiley B, Sun Y, Xia Y (2005) Langmuir 21:8077–8080
34. Sun Y, Xia Y (2002) Adv Mater 14:833–837
35. Korte KE, Skrabalak SE, Xia Y (2008) J Mater Chem 18:437–441
36. Dong X, Ji X, Wu H, Zhao L, Li J, Yang W (2009) J Phys Chem C 113:6573–6576
37. Caswell KK, Bender CM, Murphy CJ (2003) Nano Lett 3:667–669
38. Sun F, Li L, Liu P, Lian Y (2011) Electroanalysis 23:395–401
39. Male KB, Hrapovic S, Liu Y, Wang D, Luong JHT (2004) Anal Chim Acta 516:35–41
40. Li X, Zhu Q, Tong S, Wang W, Song W (2009) Sens Actuators B 136:444–450
41. Yang J, Zhang W-D, Gunasekaran S (2010) Biosens Bioelectron 26:279–284
42. Huang T-K, Lin K-W, Tung S-P, Cheng T-M, Chang IC, Hsieh Y-Z, Lee C-Y, Chiu H-T (2009) J Electroanal Chem 636:123–127
43. Wang G, Wei Y, Zhang W, Zhang X, Fang B, Wang L (2010) Microchim Acta 168:87–92
44. Kang X, Mai Z, Zou X, Cai P, Mo J (2007) Anal Biochem 363:143–150
45. Kumar SA, Cheng H-W, Chen S-M, Wang S-F (2010) Mater Sci Eng C 30:86–91